Biodistribution and Radiation Dosimetry of ^{11}C-Nicotine from Whole-Body PET Imaging in Humans

Pradeep K. Garg, Stephen J. Lokitz, Rachid Nazih, and Sudha Garg

Department of Radiology, Wake Forest University Health Sciences, Winston Salem, North Carolina; and Biomedical Research Foundation, Shreveport, Louisiana

This study assessed the in vivo distribution of ^{11}C-nicotine and the absorbed radiation dose from whole-body ^{11}C-nicotine PET imaging of 11 healthy (5 male and 6 female) subjects. **Methods:** After an initial CT attenuation scan, ^{11}C-nicotine was administered via intravenous injection. A dynamic PET scan was acquired for 90 s with the brain in the field of view, followed by a series of 13 whole-body PET scans acquired over a 90-min period. Regions of interest were drawn over organs visible in the reconstructed PET images. Time–activity curves were generated, and the residence times were calculated. The absorbed radiation dose for the whole body was calculated by entering the residence time in OLINDA/EXM 1.0 software to model the equivalent organ dose and the effective dose for a 70-kg man. **Results:** The mean residence times for ^{11}C-nicotine in the liver, red marrow, brain, and lungs were 0.048 ± 0.010, 0.031 ± 0.005, 0.021 ± 0.004, and 0.020 ± 0.005 h, respectively. The mean effective dose for ^{11}C-nicotine was 5.44 ± 0.67 μSv/MBq. The organs receiving the highest absorbed dose from the ^{11}C-nicotine injection were the urinary bladder wall (14.68 ± 8.70 μSv/MBq), kidneys (9.56 ± 2.46 μSv/MBq), liver (8.94 ± 1.67 μSv/MBq), and spleen (9.49 ± 3.89 μSv/MBq). The renal and hepatobiliary systems were the major clearance and excretion routes for radioactivity. **Conclusion:** The estimated radiation dose from ^{11}C-nicotine administration is relatively modest and would allow for multiple PET examinations on the same subject.

Key Words: ^{11}C nicotine; radiation absorbed dose; PET dosimetry; whole-body PET imaging

J Nucl Med 2017; 58:473–478
DOI: 10.2967/jnumed.116.180059

The rate of smoking by adults has decreased substantially in the United States since the hallmark 1964 U.S. Surgeon General's report. Nonetheless, 40 million Americans still smoke regularly, and approximately 400,000 people die each year from illnesses directly associated with smoking (*1*). Although the various components of tobacco cause different effects, nicotine has been identified as one of the primary chemicals responsible for tobacco addiction in humans (*2,3*). More recently, there has been a steady rise in the use of newly developed nicotine delivery devices (such as e-cigarettes) to replace cigarettes, and their use has now surpassed that of any other tobacco product, especially among high-school students (*4*). There is growing concern among the scientific, medical, and regulatory communities over the deleterious impact of nicotine consumption on human health. Aside from the reinforcing action, nicotine perpetuates the smoking habit in humans through the aversive consequences of nicotine withdrawal, a negative reinforcement phenomenon (*5–7*). Neuronal nicotinic acetylcholine receptors have been identified as one of the primary sites of action in the brain for the elicitation of reinforcing effects, dependency, and withdrawal expressions during cessation of smoking (*8–12*). PET imaging is highly useful for studying the impact of smoking and the targeting of acetylcholine receptor systems. The involvement of nicotinic receptors in brain cholinergic transmission alludes to the role of nicotine in Alzheimer disease, in which a direct relationship exists between nicotinic receptors, cholinergic transmission, and pathologic symptoms (*13–15*). A PET imaging study in patients with neurodegenerative disease showed significantly reduced uptake of ^{11}C-nicotine in Alzheimer disease patients in comparison with healthy controls, especially in the frontal and temporal cortices (*16–18*), a finding that is in accordance with the strong correlation between nicotine binding in the parietal cortex and performance in a visuospatial ability test (*16*). ^{11}C-nicotine PET has also been useful for investigating the impact of menthol in cigarettes, which can alter nicotine accumulation in the brain (*19*). A ^{11}C-nicotine PET study we performed earlier showed a slow accumulation of nicotine in the brains of dependent smokers, which was partially due to a slower release of accumulated nicotine in the lungs (*20*), establishing a direct relationship between nicotine and its pharmacologic impact on human health. These imaging studies further underscore the importance of ^{11}C-nicotine PET in the study of addiction and other in vivo neurologic functions. Despite multiple publications on the use of ^{11}C-nicotine in humans, to our knowledge there are no published data on the radiation dosimetry of ^{11}C-nicotine. Therefore, the aim of this study was to obtain estimates of radiation dosimetry of ^{11}C-nicotine in humans. We report on the in vivo distribution of ^{11}C-nicotine in humans and the estimated radiation dose from whole-body ^{11}C-nicotine PET scans.

MATERIALS AND METHODS

Subjects

This study was approved by the Radiation Safety Committee and the Institutional Review Board of the Wake Forest University Medical Center. Written informed consent was obtained from each participant before the PET studies. In total, 11 (5 male and 6 female) healthy nonsmokers (mean age ± SD, 39.1 ± 9.1 y) with an average weight of 80.3 ± 26.3 kg were enrolled.

Synthesis of ^{11}C-Nicotine Radiochemistry

^{11}C-nicotine was produced via *N*-methylation of (*S*)-nornicotine using ^{11}C-methyltriflate prepared by a previously reported method

Received Jun. 23, 2016; revision accepted Aug. 28, 2016.
For correspondence or reprints contact: Pradeep K. Garg, Center for Molecular Imaging and Therapy, P.O. Box 38050, Shreveport, LA 71103.
E-mail: pgarg@biomed.org
Published online Sep. 22, 2016.

with minor modifications (*21*). Briefly, ^{11}C-methyltriflate (FXc-Pro module; GE Healthcare) was bubbled through a solution of 0.25 mg of (*S*)-nor-nicotine biscamsylate and 10 μL of a 5% solution of 1,2,2,6,6-pentamethyl piperidine in acetonitrile. After the ^{11}C-methyltriflate delivery was complete, the reaction mixture was loaded on the high-performance liquid chromatography loop and the desired product was isolated using a semipreparatory high-performance liquid chromatography column (μPorasil silica, 7.8 × 300 mm, 10 μm; Waters) eluted with 96% dichloromethane and 4% methanol/trimethylamine (100/1, v/v), at a flow rate of 2 mL/min.

PET Imaging

The PET/CT images were acquired on a Discovery VCT PET/CT scanner (GE Healthcare). The imaging characteristics of this scanner have been described previously (*22*). Iterative image reconstruction with measured attenuation correction, modeled scatter correction, and random correction using singles counting rates was performed for all subjects (*23*). Data acquired from image sets in counts per pixel were calibrated using the standard quantification procedures to report uptake values in Bq/cc.

The subjects were positioned on the scanner bed, and a whole-body (top of the head to toes) CT scan was acquired for attenuation correction and localization of organs. Subsequently, 505 ± 96 MBq (13.6 ± 2.6 mCi) of ^{11}C-nicotine were injected intravenously into the subject's arm, and sequential PET scans were acquired in 3-dimensional mode over 90 min to provide a total of 14 scans (time points). Before the first whole-body PET scan, dynamic brain scans were acquired for the first 90 s commencing from the time of ^{11}C injection (45 frames, 2 s each), to capture the uptake and distribution characteristics of ^{11}C-nicotine in the brain. Subsequently, 12 whole-body image sets (head to midthigh) were obtained using the following image acquisition sequence: 2 × 15 s, 3 × 20 s, 2 × 30 s, 3 × 60 s, and 2 × 90 s. After the twelfth whole-body scan, a final image set covering the entire body from the top of the head to the toes was acquired (60 s/bed position). The PET images were reconstructed using fully 3-dimensional maximum-likelihood ordered-subset expectation maximization, with 28 subsets, 2 iterations, and a 6-mm postloop filter (*23*).

PET Image Analysis and Calculation of Residence Time

Reconstructed coronal images were used to identify and measure the radioactivity content in key organs. Using PMOD 3.2 software (PMOD Technologies), regions of interest (ROIs) were drawn manually across all image planes, for each image set, to determine total radioactivity accumulated in an organ. All ROIs were carefully drawn to minimize organ-boundary edge artifacts and were viewed in coronal, sagittal, and axial directions to ensure that different ROIs did not overlap. The CT images were used for secondary confirmation of the anatomic accuracy of the PET ROIs. Lumbar spine ROIs were used to calculate radioactivity in the red marrow. The guidelines of International Commission on Radiological Protection publication 89 (*24*) were followed to estimate the quantity of red marrow in an adult and to calculate the total amount of radioactivity accumulated in the bone marrow. Whole-body muscle uptake was calculated by multiplying the quantity of radioactivity present in a thigh muscle ROI by a weighting factor, as described in following equation:

$$\%ID_{muscle} = \%ID_{thigh\ muscle\ ROI} \times \frac{weight \times \%muscle\ mass}{vol_{thigh\ muscle\ ROI} \times \rho_{muscle}}.$$

Additionally, a large ROI was created to calculate the quantity of radioactivity in the whole body. Time–activity curves were generated from each ROI, and the accumulated radioactivity in each organ was expressed as percentage injected dose (%ID). For residence time calculations, the radioactivity content beyond the last imaged time-point was assumed to be depleted exclusively by physical decay of the radioactivity. Integration of the time–activity curve data from time zero to complete elimination of radioactivity (area under the curve) was performed using the trapezoidal method to derive residence times for various organs.

Calculation of Equivalent Organ Dose and Effective Dose

The absorbed radiation dose for individual organs was estimated by entering organ residence times into OLINDA/EXM 1.0 software (*25*). OLINDA uses the MIRD scheme, and the dose estimates were obtained for the 70-kg adult man. Effective dose equivalent and absorbed radiation dose were determined using the methods published in the earlier International Commission on Radiological Protection publications, 30 and 60, respectively (*26,27*).

RESULTS

The ^{11}C-nicotine was eluted from a semipreparatory high-performance liquid chromatography column in about 6.5–8.5 min with a radiochemical yield of about 30% and a radiochemical purity of more than 99%. The product was reconstituted in saline for injection and sterile-filtered using a 0.2-μm Millipore filter. The average specific activity (n = 16) of ^{11}C-nicotine was 264 ± 23 TBq/mmol (7,158 ± 648 Ci/mmol) at the end of synthesis.

After intravenous injection, the radioactivity accumulated in the brain rapidly. Representative brain PET images from one male and one female subject are shown in Figure 1. The time–activity curves generated from the brain images acquired during the first 90 s for representative male and female subjects are shown in Figure 2. In general, a lag of about 8–10 s between the time of injection and the arrival of radioactivity in the brain was noted. Comparing the radioactivity levels from the brain time–activity curves of the representative male and female subjects, higher levels of radioactivity were noted in the female brains (Fig. 2). Besides the accumulation levels, these time–activity curves also show a distinct difference in the rate of radioactivity accumulation between the male and female brains. The uptake slope during the initial phase (5–37 s) of radioactivity accumulation in the female

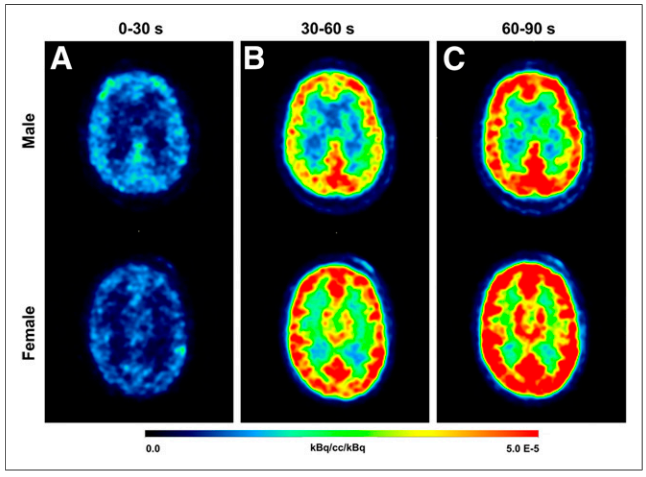

FIGURE 1. Axial view of representative brain PET images from one man (top) and one woman (bottom). PET scans were acquired dynamically over 90 s (45 frames of 2 s each) after injection of ^{11}C-nicotine. Data are normalized to injected dose. These 45 frames were divided into 3 sets: 0–30 s (A), 30–60 s (B), and 60–90 s (C). A higher accumulation was seen in female brain than in male brain (B and C).

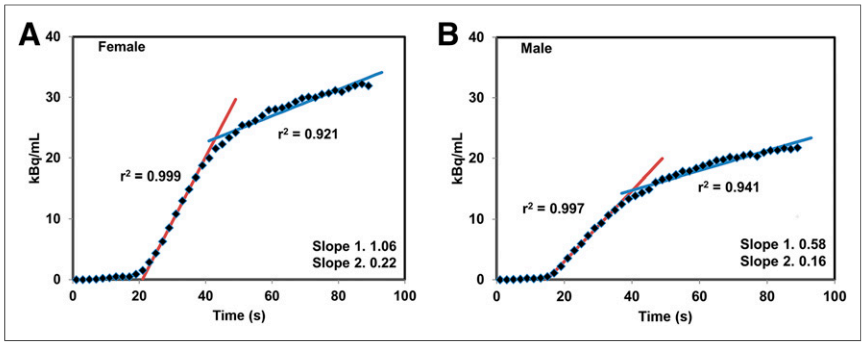

FIGURE 2. Time–activity curves generated from dynamic brain PET scans acquired over first 90 s for representative woman (A) and man (B). After initial lag of about 10 s between injection and arrival of radioactivity in brain, rapidly increasing levels were noted in brain for both groups. These time–activity curves show initial faster radioactivity accumulation phase (red line) followed by much slower but sustained accumulation phase (blue line).

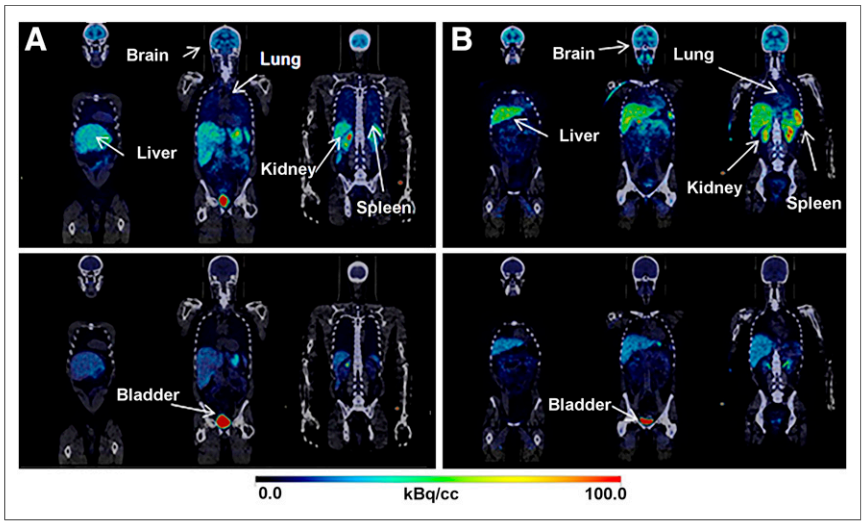

FIGURE 3. Coronal view of representative 2.8-min (top) and 22.6-min (bottom) whole-body PET/CT images of man (A) and woman (B). Early images clearly delineate brain, liver, spleen, lungs, and kidneys. Late images show intense accumulation in urinary bladder. Brain, liver, lungs, spleen, and kidneys are less conspicuous in late images than in early images, indicating significant washout of radioactivity from these organs with time.

and male brain was 1.06 (linear fit $r^2 = 0.999$) and 0.58 (linear fit $r^2 = 0.997$), respectively ($P < 0.001$). This initial rapid rise in radioactivity was followed by a much slower accumulation phase. The average slope during this slow uptake period was 0.22 ($r^2 = 0.921$) and 0.16 ($r^2 = 0.941$) in the female and male brains, respectively.

The whole-body PET images show a rapid uptake and distribution of ^{11}C-nicotine for most major organs. Dividing the whole-body ROI value by the decay-corrected injected dose provided a recovery coefficient of 95% ± 7%. PET images of representative male and female subjects showing typical whole-body distribution patterns for ^{11}C-nicotine are in Figure 3. The 2.8-min PET/CT images clearly delineated most major organs such as the brain, lungs, spleen, liver, and kidneys. Because urinary excretion was the primary route for radioactivity elimination, the urinary bladder was more distinct on the later images. Figure 4 shows uptake in the right and left lungs of representative male and female subjects and average uptake in the left and right lungs for all subjects. The time–activity curves generated for several of the major organs that were easily discernible on PET images are presented in Figure 5. As seen from Figure 5, after an initial rapid uptake, a significant washout of radioactivity was noted for most organs with time. For example, the %ID of ^{11}C in the liver, brain, red marrow, muscle, and lungs was 9.4 ± 1.9, 6.2 ± 1.5, 5.0 ± 2.0, 15.2 ± 9.1, and 6.0 ± 2.2, respectively, at 2.8 min, and these levels decreased to 0.6 ± 0.2, 0.1 ± 0.0, 0.3 ± 0.1, 1.2 ± 0.4, and 0.2 ± 0.0 by 86.5 min.

The residence time for each organ was computed by integrating the total accumulated radioactivity in the individual organ from the time of injection until complete elimination. The mean residence times for various organs are shown in Table 1. The absorbed doses for various organs were estimated by entering the residence times into the OLINDA software and are presented in Table 2. The 4 organs that received the highest absorbed dose in this study were the urinary bladder wall (14.68 ± 8.70 μSv/MBq), kidneys (9.56 ± 2.46 μSv/MBq), spleen (9.49 ± 3.89 μSv/MBq), and liver (8.94 ± 1.67 μSv/MBq). The mean effective radiation dose to a 70-kg human was 5.44 ± 0.67 μSv/MBq

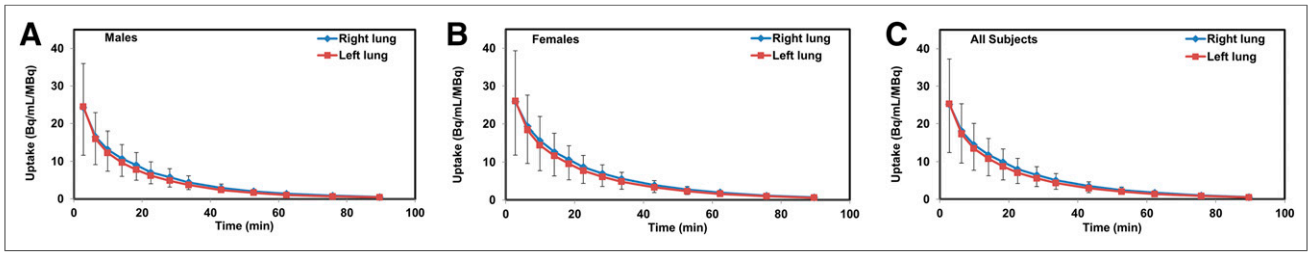

FIGURE 4. (A and B) Time–activity curves showing accumulation of ^{11}C nicotine in right and left lungs from representative man (A) and woman (B). (C) Average uptake in right and left lungs from all subjects. In all cases, slightly higher uptake was seen in right lung, but these differences were statistically insignificant ($P > 0.12$).

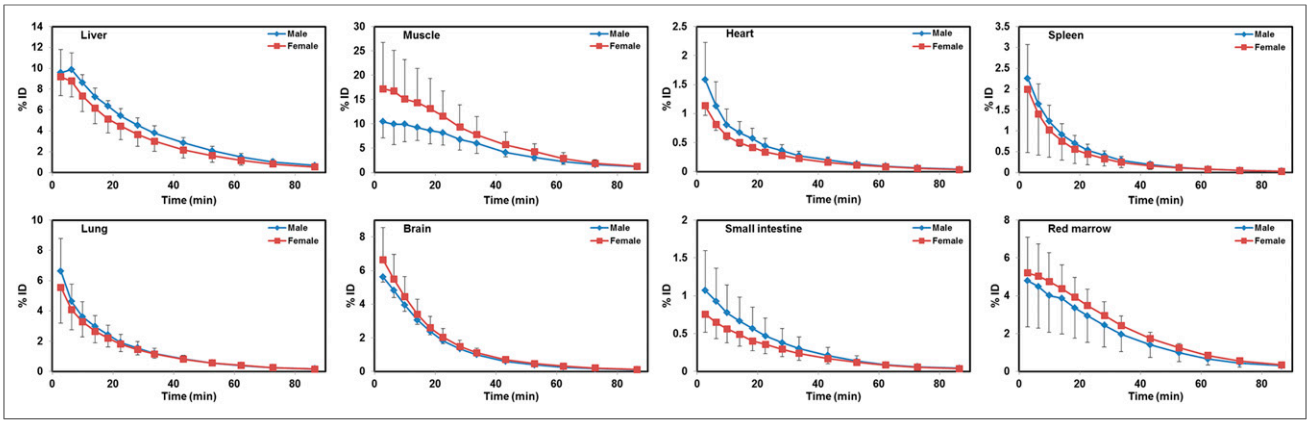

FIGURE 5. Time–activity curves generated from ROIs placed on organs that were easily discernible on whole-body PET/CT images. Radioactivity level in each organ is presented as averaged %ID for male and female groups. In general, accumulation levels in most organs peaked during first few minutes and then decreased rapidly.

(20.11 ± 2.47 mrem/mCi). The effective dose calculated in this study for ^{11}C-nicotine is similar to values reported for many of the commonly used ^{11}C-labeled radiopharmaceuticals, as shown in Table 3.

DISCUSSION

Several investigators have identified advantages to using ^{11}C-nicotine PET in the study of nicotine addiction and neurodegenerative disease. A PET imaging study showed lower accumulation of ^{11}C-nicotine in the brains of Alzheimer disease patients than in age-matched healthy controls, implying the loss of nicotinic receptors in Alzheimer disease (*28*). PET studies on patients with Alzheimer disease were also effective in finding a direct correlation between ^{11}C-nicotine levels in the parietal cortex and the results of a clock-drawing test (*16*). Another ^{11}C-nicotine PET imaging study investigated the influence of mentholated cigarettes on nicotine accumulation in the brain (*19*). These and many other imaging studies conducted over the years testify to the merits of ^{11}C-nicotine PET for a variety of applications (*19,20,29–33*). However, despite the many ^{11}C-nicotine studies performed on humans, no dosimetry data have been presented. To our knowledge, this study is the first to report on the radiation dosimetry of ^{11}C-nicotine derived from whole-body PET/CT imaging on humans.

TABLE 1
Residence Times Calculated from Whole-Body Images of 11 Subjects Injected with ^{11}C-Nicotine

Organ	Residence time (h)
Brain	0.021 ± 0.004
Liver	0.048 ± 0.010
Lung	0.020 ± 0.005
Bladder	0.019 ± 0.013
Kidney	0.009 ± 0.003
Muscle	0.088 ± 0.040
Red marrow	0.031 ± 0.005
Spleen	0.005 ± 0.003
Stomach	0.007 ± 0.004
Pancreas	0.001 ± 0.000
Heart	0.004 ± 0.001
Lower large intestine	0.005 ± 0.002
Small intestine	0.004 ± 0.002
Remainder of body	0.227 ± 0.039

Data are mean ± SD.

In this study, the PET images showed a rapid uptake of radioactivity in most organs, leading to clear visualization of several organs within a few minutes of the intravenous injection of ^{11}C-nicotine (Fig. 3). Similarly, radioactivity rapidly accumulated in the brain soon after injection (Fig. 1). The time–activity curves generated from the PET images revealed a lag of about 8–10 s between the time of injection and the arrival of radioactivity in the brain (Fig. 2). The radioactivity levels peaked in the brain within 90 s after injection, with an initial sharp rise during the first 5–37 s followed by a slow but sustained accumulation (Fig. 2). Regression analysis of the initial sharp rise showed a linear fit of data (r^2 = 0.999 for women; r^2 = 0.997 for men), whereas the later slower rise showed a nonlinear fit (r^2 = 0.921 for women; r^2 = 0.941 for men). This pattern is similar to that reported previously by ourselves and others when ^{11}C-nicotine was administered by inhalation (*20,34*).

Although the time–activity curves from the whole-body PET images showed a rapid but low uptake of ^{11}C-nicotine in major organs such as the heart, spleen, kidneys, liver, and lungs, most organs were easily delineated on the PET images (Fig. 3). Uptake in the right lung on PET images was slightly higher than that in the left lung. The time–activity curves from representative male and female subjects and from the average of all subjects indicated slightly higher but statistically insignificant levels of radioactivity accumulation in the right lung (Fig. 4). Initial uptake in the lungs was followed by a rapid and significant washout of radioactivity. Similarly, several other major organs also showed a significant and steady washout of radioactivity with time. For example, the radioactivity in the liver and kidneys peaked within the first 5 min and decreased about 15-fold by 86.5 min (Fig. 5). Similarly, the radioactivity in the blood pool was 26.1 ± 8.0 %ID at 2.78 min and decreased 45-fold to 0.6 ± 0.1 %ID by 86.5 min. Although the

TABLE 2
Radiation Dose Estimates for ^{11}C-Nicotine

Organ	Dose	
	μSv/MBq	mrem/mCi
Adrenals	2.93 ± 0.20	10.85 ± 0.72
Brain	5.33 ± 0.98	19.74 ± 3.80
Breasts	1.75 ± 0.19	6.49 ± 0.70
Gallbladder wall	3.21 ± 0.26	11.86 ± 0.96
Lower large intestine wall	6.96 ± 1.75	25.75 ± 6.47
Small intestine	3.69 ± 0.54	13.65 ± 2.01
Stomach wall	6.00 ± 1.97	22.22 ± 7.28
Upper large intestine wall	2.63 ± 0.16	9.72 ± 0.59
Heart wall	3.65 ± 0.46	13.51 ± 1.70
Kidneys	9.56 ± 2.46	35.35 ± 9.08
Liver	8.94 ± 1.67	33.03 ± 6.14
Lungs	6.22 ± 1.24	23.03 ± 4.60
Muscle	2.01 ± 0.34	7.45 ± 1.24
Ovaries	2.72 ± 0.12	10.07 ± 0.45
Pancreas	4.29 ± 0.57	15.89 ± 2.13
Red marrow	5.15 ± 0.50	19.09 ± 1.83
Osteogenic cells	4.63 ± 0.33	17.15 ± 1.21
Skin	1.53 ± 0.12	5.65 ± 0.46
Spleen	9.49 ± 3.89	35.09 ± 14.36
Testes	1.91 ± 0.11	7.06 ± 0.42
Thymus	2.07 ± 0.16	7.67 ± 0.60
Thyroid	7.14 ± 1.00	26.41 ± 3.70
Urinary bladder wall	14.68 ± 8.70	54.35 ± 32.28
Uterus	2.92 ± 0.30	10.78 ± 1.11
Total body	2.81 ± 0.04	10.40 ± 0.15
Effective dose equivalent	5.71 ± 0.73	21.13 ± 2.70
Effective dose	5.44 ± 0.67	20.11 ± 2.47

Data are mean ± SD.

muscles were not distinctly visible on the PET scans, the %ID was significantly higher in the muscles than in the liver and spleen (Fig. 5), the two tissues that were distinctly visible on the PET images. This anomaly could be due to the relatively higher mass of muscle in the human body in comparison with the mass of the liver and spleen. The bladder showed a steady rise of radioactivity with time for the duration of the scan because of renal excretion of radioactivity. Unlike the uptake pattern in the brain and muscle, some other major organs showed higher levels of ^{11}C-nicotine in men than in women (Fig. 5). Although notable, these uptake differences were statistically insignificant ($P > 0.1$).

The residence time for individual organs was calculated using the area under the time–activity curves generated for those organs from the PET images. The maximum residence time for ^{11}C-labeled radiopharmaceuticals is 0.488 h (*35*). The residence time for the remainder of the body was obtained by subtracting the sum of the residence time for all identified organs from 0.488 h.

TABLE 3
Comparison of Effective Dose Estimates Between ^{11}C-Nicotine and Other ^{11}C-Radiopharmaceuticals

Organ	^{11}C-nicotine*	^{11}C-PIB (*37*)	^{11}C-PK11195 (*35*)
Urinary bladder wall	14.7	16.6	9.8
Kidneys	9.6	12.6	14.0
Spleen	9.5	4.3	12.5
Liver	8.9	19.0	9.5
Thyroid	7.1	2.4	1.9
Effective dose	5.4	4.7	4.8

*Current study.

The residence times thus generated agreed reasonably well across subjects and were entered in the OLINDA software to derive the absorbed radiation dose for individual organs (Table 2). The estimated mean effective dose for ^{11}C-nicotine was 5.44 ± 0.67 μSv/MBq (20.11 ± 2.47 mrem/mCi) for a 70-kg human. The estimated effective dose equivalent for ^{11}C-nicotine was 5.71 ± 0.73 μSv/MBq (21.13 ± 2.70 mrem/mCi). The critical organs are the urinary bladder wall, kidneys, and spleen. On the basis of these calculated values, a standard injection of 555 MBq (15 mCi) of ^{11}C-nicotine would result in 3.02 mSv (0.3 rem) of exposure to a 70-kg human. The current federal guidelines limit the radiation exposure for a research subject to a 0.03-Sv (3-rem) effective dose for a single study and a 0.05-Sv (5-rem) effective dose for the whole year (*36*). This limit corresponds to administration of about 9,250 MBq (~250 mCi) of ^{11}C-nicotine per subject per year. These results showing that the absorbed dose from ^{11}C-nicotine in human studies is relatively low should help in planning future studies and in advising research subjects of the potential risk from the radiation associated with ^{11}C-nicotine PET studies.

CONCLUSION

We evaluated the whole-body distribution and radiation dosimetry of ^{11}C-nicotine. The effective dose of ^{11}C-nicotine in a healthy subject is 5.4 μSv/MBq, thus suggesting only a modest radiation dose from a 555-MBq (15-mCi) injection of ^{11}C-nicotine. These results will be helpful in calculating the associated radiation dose when planning multiple PET studies with ^{11}C-nicotine on the same subject.

DISCLOSURE

No potential conflict of interest relevant to this article was reported.

ACKNOWLEDGMENTS

We acknowledge the skillful assistance of the staff at Wake Forest University Health Sciences Research PET center. Support from the Center for Biomolecular Imaging is also highly appreciated.

REFERENCES

1. Jamal A, Homa DM, O'Connor E, et al. Current cigarette smoking among adults: United States, 2005-2014. *MMWR Morb Mortal Wkly Rep.* 2015;64:1233–1240.
2. Stolerman IP, Mirza NR, Shoaib M. Nicotine psychopharmacology: addiction, cognition and neuroadaptation. *Med Res Rev.* 1995;15:47–72.
3. Stolerman IP, Jarvis MJ. The scientific case that nicotine is addictive. *Psychopharmacology (Berl).* 1995;117:2–10.
4. Singh T, Arrazola RA, Corey CG. Tobacco use among middle and high school students: United States, 2011-2015. *MMWR Morb Mortal Wkly Rep.* 2016;65:361–367.
5. Doherty K, Kinnunen T, Militello FS, Garvey AJ. Urges to smoke during the first month of abstinence: relationship to relapse and predictors. *Psychopharmacology (Berl).* 1995;119:171–178.
6. George O, Ghozland S, Azar MR, et al. CRF-CRF1 system activation mediates withdrawal-induced increases in nicotine self-administration in nicotine-dependent rats. *Proc Natl Acad Sci USA.* 2007;104:17198–17203.
7. Kenny PJ, Markou A. Conditioned nicotine withdrawal profoundly decreases the activity of brain reward systems. *J Neurosci.* 2005;25:6208–6212.
8. Goldberg SR, Spealman RD, Goldberg DM. Persistent behavior at high rates maintained by intravenous self-administration of nicotine. *Science.* 1981;214: 573–575.
9. Harvey DM, Yasar S, Heishman SJ, Panlilio LV, Henningfield JE, Goldberg SR. Nicotine serves as an effective reinforcer of intravenous drug-taking behavior in human cigarette smokers. *Psychopharmacology (Berl).* 2004;175:134–142.
10. Watkins SS, Epping-Jordan MP, Koob GF, Markou A. Blockade of nicotine self-administration with nicotinic antagonists in rats. *Pharmacol Biochem Behav.* 1999;62:743–751.
11. Harrison AA, Gasparini F, Markou A. Nicotine potentiation of brain stimulation reward reversed by DH beta E and SCH 23390, but not by eticlopride, LY 314582 or MPEP in rats. *Psychopharmacology (Berl).* 2002;160:56–66.
12. Shiffman SM, Jarvik ME. Smoking withdrawal symptoms in two weeks of abstinence. *Psychopharmacology (Berl).* 1976;50:35–39.
13. Struble RG, Cork LC, Whitehouse PJ, Price DL. Cholinergic innervation in neuritic plaques. *Science.* 1982;216:413–415.
14. Warpman U, Nordberg A. Epibatidine and ABT 418 reveal selective losses of alpha 4 beta 2 nicotinic receptors in Alzheimer brains. *Neuroreport.* 1995;6: 2419–2423.
15. Perry E, Martin-Ruiz C, Lee M, et al. Nicotinic receptor subtypes in human brain ageing, Alzheimer and Lewy body diseases. *Eur J Pharmacol.* 2000;393:215–222.
16. Kadir A, Almkvist O, Wall A, Langstrom B, Nordberg A. PET imaging of cortical ^{11}C-nicotine binding correlates with the cognitive function of attention in Alzheimer's disease. *Psychopharmacology (Berl).* 2006;188:509–520.
17. Nordberg A. PET studies and cholinergic therapy in Alzheimer's disease. *Rev Neurol (Paris).* 1999;155(suppl 4):S53–S63.
18. Nordberg A. Nicotinic receptor abnormalities of Alzheimer's disease: therapeutic implications. *Biol Psychiatry.* 2001;49:200–210.
19. Zuo Y, Mukhin AG, Garg S, et al. Sex-specific effects of cigarette mentholation on brain nicotine accumulation and smoking behavior. *Neuropsychopharmacology.* 2015;40:884–892.
20. Rose JE, Mukhin AG, Lokitz SJ, et al. Kinetics of brain nicotine accumulation in dependent and nondependent smokers assessed with PET and cigarettes containing ^{11}C-nicotine. *Proc Natl Acad Sci USA.* 2010;107:5190–5195.
21. Halldin C, Nagren K, Swahn CG, Langstrom B, Nyback H. (S)- and (R)-[^{11}C] nicotine and the metabolite (R/S)-[^{11}C]cotinine: preparation, metabolite studies and in vivo distribution in the human brain using PET. *Int J Rad Appl Instrum B.* 1992;19:871–880.
22. Teräs M, Tolvanen T, Johansson JJ, Williams JJ, Knuuti J. Performance of the new generation of whole-body PET/CT scanners: Discovery STE and Discovery VCT. *Eur J Nucl Med Mol Imaging.* 2007;34:1683–1692.
23. Iatrou M, Ross SG, Manjeshwar R, Stearns CW. A fully 3D iterative image reconstruction algorithm incorporating data correction. *Nuclear Science Symposium Conference Record.* 2004;4:2493–2497.
24.. Basic anatomical and physiological data for use in radiological protection: reference values—a report of age- and gender-related differences in the anatomical and physiological characteristics of reference individuals. ICRP publication 89. *Ann ICRP.* 2002;32:5–265.
25. Stabin MG, Sparks RB, Crowe E. OLINDA/EXM: the second-generation personal computer software for internal dose assessment in nuclear medicine. *J Nucl Med.* 2005;46:1023–1027.
26. ICRP-30: limit for intakes of radionuclides by workers. *Ann ICRP.* 1981;6:1–124.
27. ICRP-60: 1990 recommendations of the International Commission on Radiological Protection. *Ann ICRP.* 1991;21:1–201.
28. Nordberg A, Hartvig P, Lilja A, et al. Decreased uptake and binding of ^{11}C-nicotine in brain of Alzheimer patients as visualized by positron emission tomography. *J Neural Transm Park Dis Dement Sect.* 1990;2:215–224.
29. Nybäck H, Halldin C, Ahlin A, Curvall M, Eriksson L. PET studies of the uptake of (*S*)- and (*R*)-[^{11}C]nicotine in the human brain: difficulties in visualizing specific receptor binding in vivo. *Psychopharmacology (Berl).* 1994;115:31–36.
30. Sharma A, Brody AL. In vivo brain imaging of human exposure to nicotine and tobacco. *Handb Exp Pharmacol.* 2009;(192):145–171.
31. Lundqvist H, Langstrom B, Nordberg A. Use of carbon-11 nicotine in PET studies. *Eur J Nucl Med.* 1997;24:825–826.
32. Lerner-Marmarosh N, Carroll FI, Abood LG. Antagonism of nicotine's action by cocaine analogs. *Life Sci.* 1995;56:PL67–PL70.
33. Muzic RF Jr, Berridge MS, Friedland RP, Zhu N, Nelson AD. PET quantification of specific binding of carbon-11 nicotine in human brain. *J Nucl Med.* 1998; 39:2048–2054.
34. Berridge MS, Apana SM, Nagano KK, Berridge CE, Leisure GP, Boswell MV. Smoking produces rapid rise of [^{11}C]nicotine in human brain. *Psychopharmacology (Berl).* 2010;209:383–394.
35. Hirvonen J, Roivainen A, Virta J, Helin S, Nagren K, Rinne JO. Human biodistribution and radiation dosimetry of ^{11}C-(R)-PK11195, the prototypic PET ligand to image inflammation. *Eur J Nucl Med Mol Imaging.* 2010;37:606–612.
36. ICRP-1996: radiological protection and safety in medicine. *Ann ICRP.* 1996; 73:26.
37. Scheinin NM, Tolvanen TK, Wilson IA, Arponen EM, Nagren KA, Rinne JO. Biodistribution and radiation dosimetry of the amyloid imaging agent ^{11}C-PIB in humans. *J Nucl Med.* 2007;48:128–133.